INTERNATIONAL JOURNAL OF CLIMATOLOGY
Int. J. Climatol. (2008)
Published online in Wiley InterScience
(www.interscience.wiley.com) DOI: 10.1002/joc.1755

RMetS
Royal Meteorological Society

The coupled seasonal hindcasts of the South American monsoon

Vasubandhu Misra[1]* and L. Marx[2]

[1] *Department of Meteorology, Florida State University, 404 Love Building, Tallahassee, FL 32306 Center for Ocean-Atmospheric Studies, Florida State University, 200 RM Johnson, Bldg., Tallahassee, FL 32306-2840*

[2] *Center for Ocean-Land-Atmosphere Studies Institute of Global Environment and Society, Inc. 4041 Powder Mill Road, Suite 302 Calverton, MD 20705*

ABSTRACT: A small set of seasonal hindcasts of the South American monsoon (SAM) from the Center for Ocean-Land-Atmosphere Studies (COLA) climate model is compared with a multi-decadal integration from the same model. It is shown that there are broad similarities in the December-January-February mean precipitation bias over continental South America, which comprise of the dry (wet) bias over central Amazon, northern South America (central Andes and south-east Brazil) in the seasonal hindcasts and in the long-term simulation. Furthermore, both types of model integrations underestimate (overestimate) the strong (weak) precipitation events over the core region of the SAM. In terms of interannual variability, seasonal hindcasts and the multi-decadal simulation show reasonably similar results. However, the spin-down of the moisture field in the seasonal hindcasts is evident in its distribution of the daily precipitation over the SAM core region. It is also found that in the multi-decadal integration owing to model drift, the Sea Surface Temperature (SST) gradient in the Atlantic Ocean north of the equator is so reduced that results in a weaker low-level cross-equatorial flow into the SAM region compared to either the seasonal hindcasts or the National Centers for Environmental Prediction (NCEP) reanalysis.

We then repeated the coupled seasonal hindcasts separately with higher horizontal and vertical resolutions of the atmospheric general circulation model (AGCM) to assess their impact on the SAM climate and its variations. It is shown that a higher horizontal resolution does not significantly improve the precipitation climatology and its interannual variability over continental South America. However, there are some marginal improvements in the frequency of occurrence of heavy precipitation events in the core region of the SAM at higher horizontal resolutions. The higher vertical resolution of the AGCM did not show a comparable benefit as the higher horizontal resolution on the SAM precipitation. However, some of the largest precipitation errors, especially over the north-eastern part of continental South America, over the Atlantic inter-tropical convergence zone and over the central Andes remain in all resolution experiments conducted in this study. Copyright © 2008 Royal Meteorological Society

KEY WORDS South American monsoon; ENSO; prediction

Received 5 November 2007; Revised 8 July 2008; Accepted 10 July 2008

1. Introduction

The seasonal prediction of the South American monsoon (SAM) is of immense importance to society at large. The core region of the SAM (5–20°S, 40–60°W) following Vera *et al.* (2006) and Grimm *et al.* (2005), is one of the leading producers of cash crops such as soybean and corn (Sampaio 2005) and it sustains a large population and generates considerable hyrdoelectrical power (Nobre *et al.*, 2006). Although north-east Brazil (or Nordeste) is well known for its seasonal climate predictability (Folland *et al.*, 2001; Misra, 2004, 2006), the SAM region is one of the more difficult regions to make reliable seasonal predictions (Nobre *et al.*, 2006). The SAM region has a robust annual cycle of precipitation (Grimm *et al.*, 2005; Vera *et al.*, 2006) that is comparable to other monsoon systems. However, its relationship to El Niño–Southern Oscillation (ENSO) variability is not uniform either spatially or during the season (Grimm, 2003, 2004), but Liebmann *et al.* (2001); Carvalho *et al.* (2004) point to a stronger influence of ENSO on extreme events over south-east Brazil through tropical–extratropical interactions. The dominant interannual variations over tropical and subtropical South America are forced by the ENSO variations in the tropical Pacific Ocean (Grimm *et al.*, 2000; Nogues-Paegle and Mo, 2002; Grimm, 2003, 2004). In recent studies (Chaves and Nobre, 2004; Nobre *et al.*, 2006), it is indicated that coupled air–sea interactions are important for realistic simulation of the variability of the SAM. These studies clearly make a persuasive argument that coupled ocean–atmosphere models are a necessary tool to resolve the interannual variability of the SAM. The negative correlation between the precipitation and *in situ* SST over the South Atlantic Convergence Zone (SACZ; the oceanic extension from the core region of SAM) is best captured in modelling frameworks that allow for coupling of the atmospheric general circulation

* Correspondence to: Vasubandhu Misra, Dept. of Meteorology, Florida State University, 404 Love Bldg., Tallahassee, FL 32306.
E-mail: vmisra@fsu.edu

model (AGCM) with an ocean general circulation model (OGCM; Nobre *et al*., 2006).

The intent of the paper is two-fold. One is to investigate how large an impact is the coupled model drift over the SAM region. The other is to determine the impact of the resolution of the AGCM on the coupled seasonal hindcasts of the SAM. Several studies in the past examining the sensitivity of the AGCM resolution on climate simulation used observed SST as the boundary forcing (Brankovic and Gregory, 2004; Duffy *et al*., 2003; Kobayashi and Sugi, 2004; Hack *et al*., 2006). In this study, we examine a similar sensitivity to AGCM resolution both in the vertical and horizontal when coupled to a given fixed resolution of an OGCM. The motivation to conduct such a resolution study with a focus on the SAM is based on the prevalence of the steep orography of the Andes and the Brazilian highlands in central-east Brazil and its influence on the climate of continental South America (Misra *et al*., 2002; Vernekar *et al*., 2003; Grimm *et al*., 2007). In a related study, Duffy *et al*. (2003) showed that a higher-resolution AGCM forced with observed SST verified the present climate simulation better than the coarser versions of the same model. In another such horizontal sensitivity study, Brankovic and Gregory (2004) indicated that no dramatic changes were found in the ensemble mean quantities between the various resolutions that they tested. They also showed that the highest model resolution does not always give the best results. Furthermore, they indicate that not all differences can be attributed to local orographic features.

The motivation to examine the sensitivity to vertical resolution of the AGCM stems from two recent developments. The National Centers for Environmental Prediction (NCEP)-Climate Forecast System (CFS) showed a dramatic improvement in the global climate especially in its ENSO simulation from its previous version primarily as a result of increasing the vertical resolution (Saha *et al*., 2006; personal communication 2005). In a related study, Inness *et al*. (2001) showed that by increasing the vertical resolution of the AGCM they were able to improve the Madden-Julian Oscillation (MJO). They attributed this feature to the spectrum of changing tropical cloud types from a bi-modal to a tri-modal distribution with introduction of mid-level congestus clouds in addition to the shallow and deep convective clouds in their higher vertical resolution model. The resulting cloud distribution more closely resembles observations especially during the suppressed phase of the MJO.

The paper is organized as follows. In the next section, a brief description of the model is provided. In Section 3, the details of the experiments conducted in this study are explained followed by a discussion of the results in Section 4. Concluding remarks are provided in Section 5.

2. Model description

The Center for Ocean-Land-Atmosphere Studies (COLA) coupled climate model (Misra *et al*., 2007) is used in this study. It comprises of the AGCM version 3.2 at a spectral resolution of T62 with 28 sigma ($= \frac{p}{p_s}$)levels which are identical to the NCEP-NCAR reanalysis model (Kalnay *et al*., 1996). The dynamical core follows from the Eulerian core of the Community Climate Model Version 3 (Kiehl *et al*., 1998) wherein the dependent variables are spectrally treated except for moisture which is advected by semi-Lagrangian scheme. The relaxed Arakawa-Schubert scheme (Bacmeister *et al*., 2000) is used for deep convective parameterization. The longwave and short-wave radiation scheme are identical to

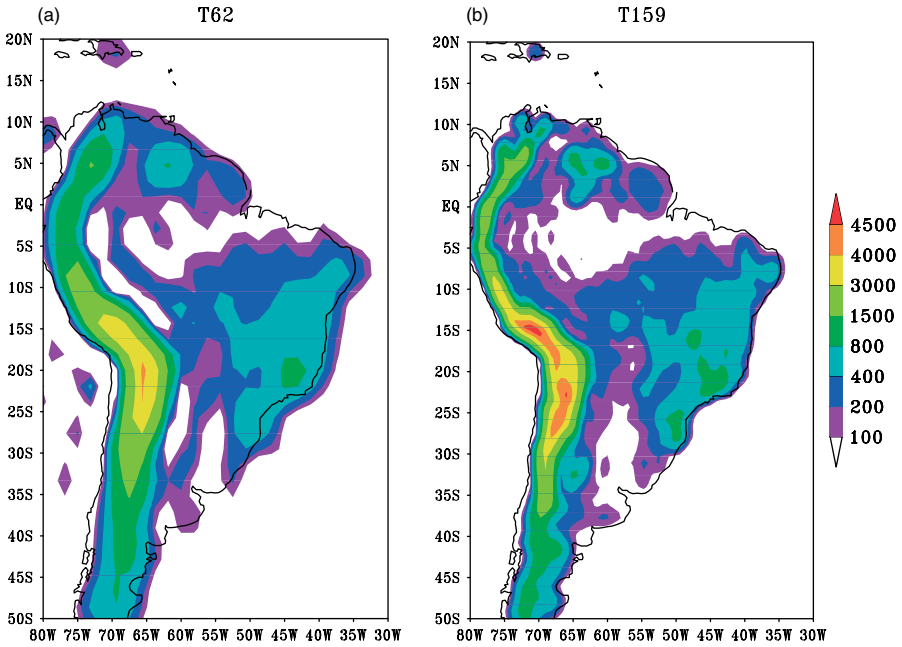

Figure 1. The model orography used at (a) T62 and (b) T159 spectral truncation. Units are in metres. This figure is available in colour online at www.interscience.wiley.com/ijoc

DOI: 10.1002/joc

those in the Community Climate System Model Version 3.0 (Collins *et al*., 2006). The cloud optical properties follow from Kiehl *et al*. (1998). The planetary boundary layer is a non-local scheme (Hong and Pan, 1996) and the shallow convection uses the formulation in Tiedtke (1984). The land surface scheme uses the simplified simple biosphere scheme (SSiB; Xue *et al*., 1991, 1996; Dirmeyer and Zeng, 1999). The time step of the AGCM is 20 min.

This COLA AGCM is coupled to the modular ocean model version 3.0 (MOM3; Pacanowski and Griffies, 1998). MOM3 covers the global oceans between 74°S and 65°N with realistic bottom topography. However, ocean depths less than 100 m are set to 100 m, and the maximum depth is 6000 m. This version of MOM3 uses the free surface method for solving the baroclinic and tracer equations. The artificial high-latitude zonal boundaries are impermeable and insulating. It has a uniform zonal resolution of 1.5° while the meridional resolution is 0.5° between 10°S and 10°N gradually increasing to 1.5° at 30°N and 30°S and fixed at 1.5° in the extratropics. The vertical mixing is the non-local K-profile parameterization of Large *et al*. (1994). The momentum mixing uses the space–time dependent scheme of Smagorinsky (1963); tracer mixing follows Redi (1982) and Gent and McWilliams (1990) quasi-adiabatic stirring. The time step of the OGCM is 1 h.

The coupling procedure follows an earlier version of the model (Kirtman *et al*., 2002). The AGCM-OGCM are coupled once a day. The daily averaged atmospheric fluxes computed by the AGCM are passed to the OGCM once a day where they are linearly interpolated to its grid. Likewise, the daily averaged SST from the OGCM is interpolated to the AGCM grid before it is passed to the AGCM at intervals of 1 day. No flux correction is applied at the time of coupling the AGCM and the OGCM.

This recently developed COLA-coupled climate model has been extensively used for seasonal–interannual modelling studies (Misra, 2007; Misra and Marx, 2007; Misra *et al*., 2007, 2008). It displays a reasonable mean global climate and its variability. However, some of the well-known systematic errors such as the split inter-tropical convergence zone (ITCZ) and the associated lack of stratus clouds in the eastern oceans are present.

Four different resolutions of the COLA AGCM (V3.2) are tested: T62L28, T62L64, T159L28 and T159L64. T62L28 corresponds to horizontal triangular spectral truncation of 62 waves (≈210 km) with 28 terrain sigma levels. Likewise, T159L28 corresponds to ≈ 80 km horizontal resolution. The 64 terrain-following sigma levels are identical to the NCEP-CFS. The physics and dynamics are identical in all these different resolution AGCMs. However, the second-order horizontal diffusion in the L28- and L64-level models is invoked in the upper 2 and 12 levels, respectively. The time step is also reduced from 12 min at the T62 resolution to 4 min in the T159 resolution model. The model orography also changes from the T62 spectral resolution to the T159 resolution as illustrated in Figure 1. The ocean model is identical for all the model runs conducted in this study.

3. Design of experiments

Several sets of integrations with the COLA-coupled climate model were conducted for this study: one long-term integration (the coupled model simulation, CMS), and several coupled dynamical seasonal predictions (CDSP). As most of the comparisons involve the CMS and the CDSP with the same resolution (T62 spectral truncation in the horizontal and 28 levels in the vertical, T62l28), this seasonal hindcast experiment is simply named CDSP. The other sensitivity seasonal hindcast runs are named after their resolution. All these experiments are briefly outlined in Table 1. For CMS, the initial conditions of the ocean and atmosphere were borrowed from the restart files of a previous multi-decadal coupled integration. Therefore, the initial conditions of the ocean are well spun-up, and the tropical upper ocean has no trends (not shown). The seasonal hindcasts in this study are integrated through a period of 1 year with the start dates of their integration of 1 December at 0000 UTC of 1982, 1988, 1997 and 1998. The choice of these times for initialization of the coupled seasonal hindcasts is deliberate, to capture the strong ENSO forcing at its most mature phase, when coupled models display their best skill (Kirtman, 2003; Jin *et al*. (2008)). For each year, ten ensemble members of the coupled model are integrated. For all coupled seasonal hindcast experiments, the initial conditions of the ocean and land are identical for a given year. They differ only in their initial conditions of the atmosphere. The initial conditions of the atmosphere are generated by running the AGCM only, for a period of 1 week with optimally interpolated SST version 2 (Reynolds *et al*., 2002) and resetting the date at the end of the 1-week-integration in its restart file to

Table I. A brief outline of the coupled model experiments.

Experiment name	Horizontal resolution	No. of Vertical levels	Length of integration (in years)	No. of ensemble members	No. of years
CMS	T62 (≈210 km)	28	40	1	40
CDSP	T62 (≈210 km)	28	1	10	4
T62L64	T62 (≈210 km)	64	1	10	4
T159L28	T159 (≈80 km)	28	1	10	4
T159L64	T159 (≈80 km)	64	1	6	4

DOI: 10.1002/joc

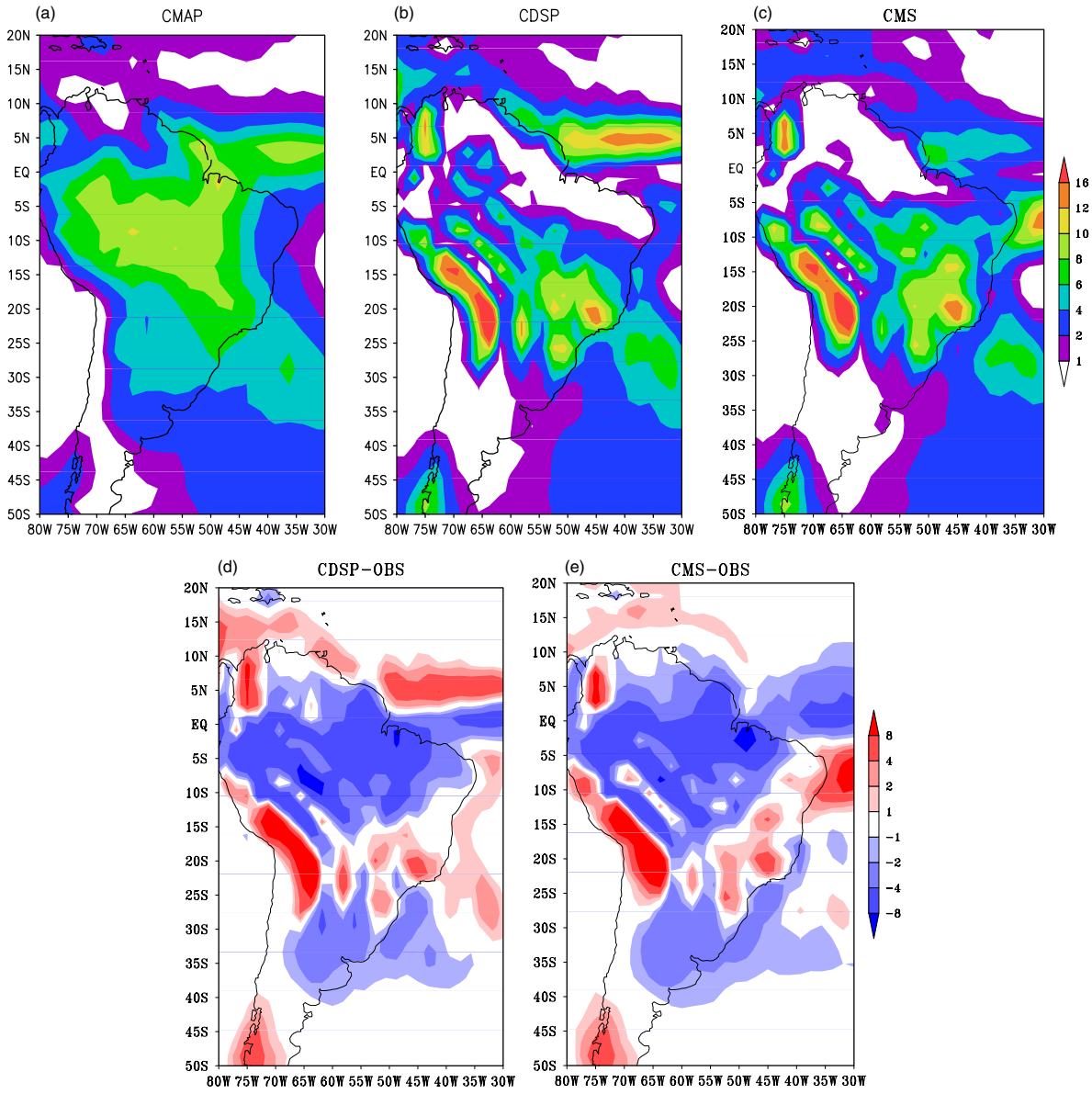

Figure 2. The climatological mean DJF precipitation from (a) OBS (CMAP), (b) CDSP and (c) CMS model runs. The corresponding mean (d) errors of CDSP computed as the difference from OBS for the same years (1982–83, 1988–89, 1997–98, and 1998–99) and (e) bias of CMS computed as the difference from a comparable long-term mean (26 year, 1979–2005) of the OBS. The Units are in mm day^{-1}. This figure is available in colour online at www.interscience.wiley.com/ijoc

the initial date of the coupled integration (1 December 0000 UTC of the given year). This is recursively done for ten times to generate ten synoptically independent initial conditions of the atmosphere for each year. This procedure was developed by Kirtman *et al.* (2002) for generating very large ensembles. The initial state of the land for the start date of the coupled integration is from an off-line data assimilation (Dirmeyer *et al.*, 2006). For the T159L64 case, only six members are generated (for reasons of limited computational resources).

The initial conditions of the ocean for the retrospective predictions were interpolated to the ocean model grid following Kirtman (2003) from the ocean data assimilation (ODA; Rosati *et al.*, 1997). The ODA was generated from a higher-resolution MOM3 with identical physics and parameter settings.

The retrospective seasonal predictions were limited to 40 seasonal hindcasts per model owing to limited computational resources. For example, 1 min of wall clock time was needed to complete 1 day of coupled integration with T62L28 using 20 processors of SGI Altix 3700. On the other hand, it required 16 min per day of coupled integration at T159L64 using 80 processors on the same SGI Altix 3700. These 40 seasonal hindcasts spanned over 4 years with ten ensemble members for each year.

4. Results

We will be primarily focussing on the rainy season of December-January-February (DJF) precipitation in the analysis of the model results. For verification, we use the monthly mean precipitation dataset from the Climate

DOI: 10.1002/joc

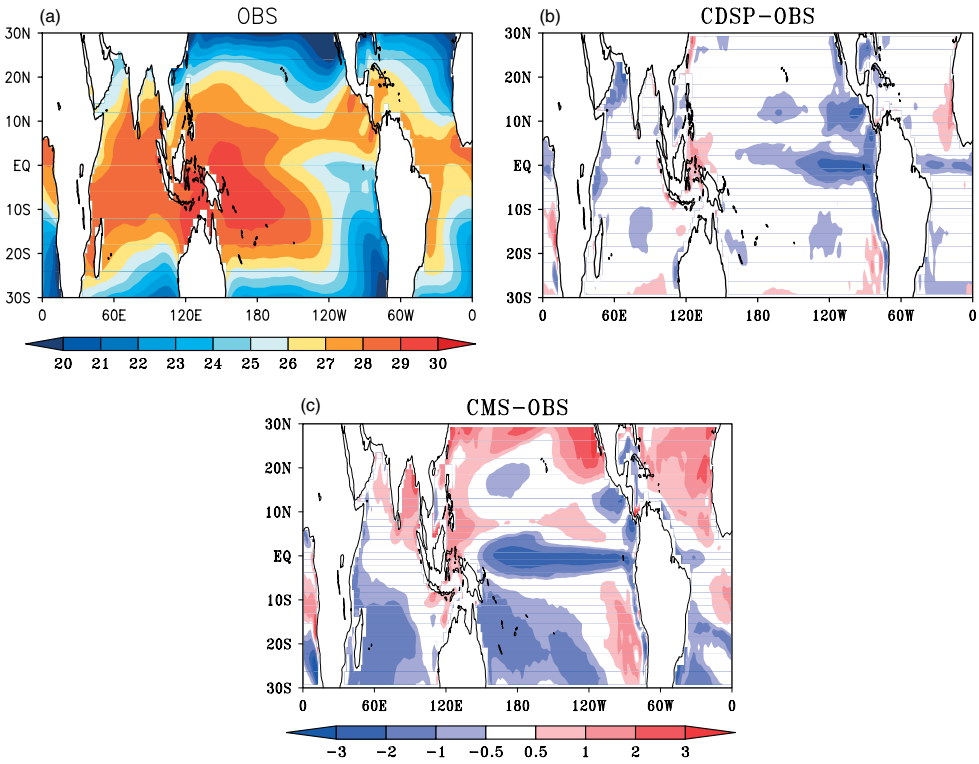

Figure 3. The climatological mean SST from (a) OBS (HADISST1.1; Rayner *et al*. 2002), (b) SST errors of CDSP computed as the difference from OBS for the same years (1982–83, 1988–89, 1997–98 and 1998–99) and (c) SST bias of CMS computed as the difference from a comparable long term mean (40 year, 1959–1998) of the OBS. Units are in mm day^{-1}. This figure is available in colour online at www.interscience.wiley.com/ijoc

Prediction Center Merged Analysis Precipitation (CMAP; Xie and Arkin, 1996) for the period 1979–2005. We supplement this with the daily precipitation dataset from rain gauges over Brazil over the 55-year period of 1950–2004 (version 19; Liebmann and Allured, 2005; hereafter rain gauge data). This dataset is gridded at 1° resolution. However, it should be noted that while computing the mean errors for the CDSP integrations we use the corresponding years of available observations, but in the case of the CMS we use a comparable number of years of observations (40; 1965–2004) to compute its difference from the observational mean. The focus of this study will be over the SAM core domain as mentioned earlier. This domain is unique in the fact that its seasonal predictability is lower than other regions of continental South America (Nobre *et al*., 2006). This primarily stems from the fact that it is also a region that has strong intra-seasonal variability (Nogues-Paegle and Mo, 1997). Nevertheless, in a recent study, Krishnamurthy and Misra (2007) point out that in years of strong ENSO variability, the domination of the seasonally persistent signal of ENSO is much stronger than that of the intra-seasonal variability. Since our seasonal hindcast runs are made when the ENSO signal is strong, our study does not delve into the intra-seasonal scales. It may, however, be pointed out that the intra-seasonal variance in the COLA model over the SAM region is relatively weak in the CMS integration.

4.1. Comparison of the seasonal hindcasts (CDSP) with the multi-decadal simulation (CMS)

4.1.1. i) Climatology

In Figure 2(a)–(c), the climatological seasonal mean DJF precipitation from the observations CMAP, CDSP and the CMS runs are shown respectively. The mean DJF precipitation errors of CDSP and the bias in CMS are shown in Figure 2(d) and (e) respectively. The common precipitation errors in CDSP and CMS integration that can be gathered from the figure are the following:

1. The dry bias over the central Amazon River Basin and the northern part of continental South America
2. The wet bias over south-east Brazil and central Andes
3. The erroneous banded structure of precipitation to the leeward side of the Andes.

There is however a major difference in the precipitation errors over the tropical Atlantic Ocean between the models. The CDSP displays a wet bias over the northern branch of the Atlantic ITCZ (north of the equator) and a dry bias over its southern branch (over and south of the equator). These errors are nearly reversed with dry and wet bias located over the northern and southern branches of the Atlantic ITCZ in the CMS integration. In addition, there are some subtle differences between the model experiments, like the dry bias over north-east Brazil is more severe in the CDSP than in the CMS experiment. It should be mentioned that the wet bias over south-east Brazil and the associated banded structure displayed both

DOI: 10.1002/joc

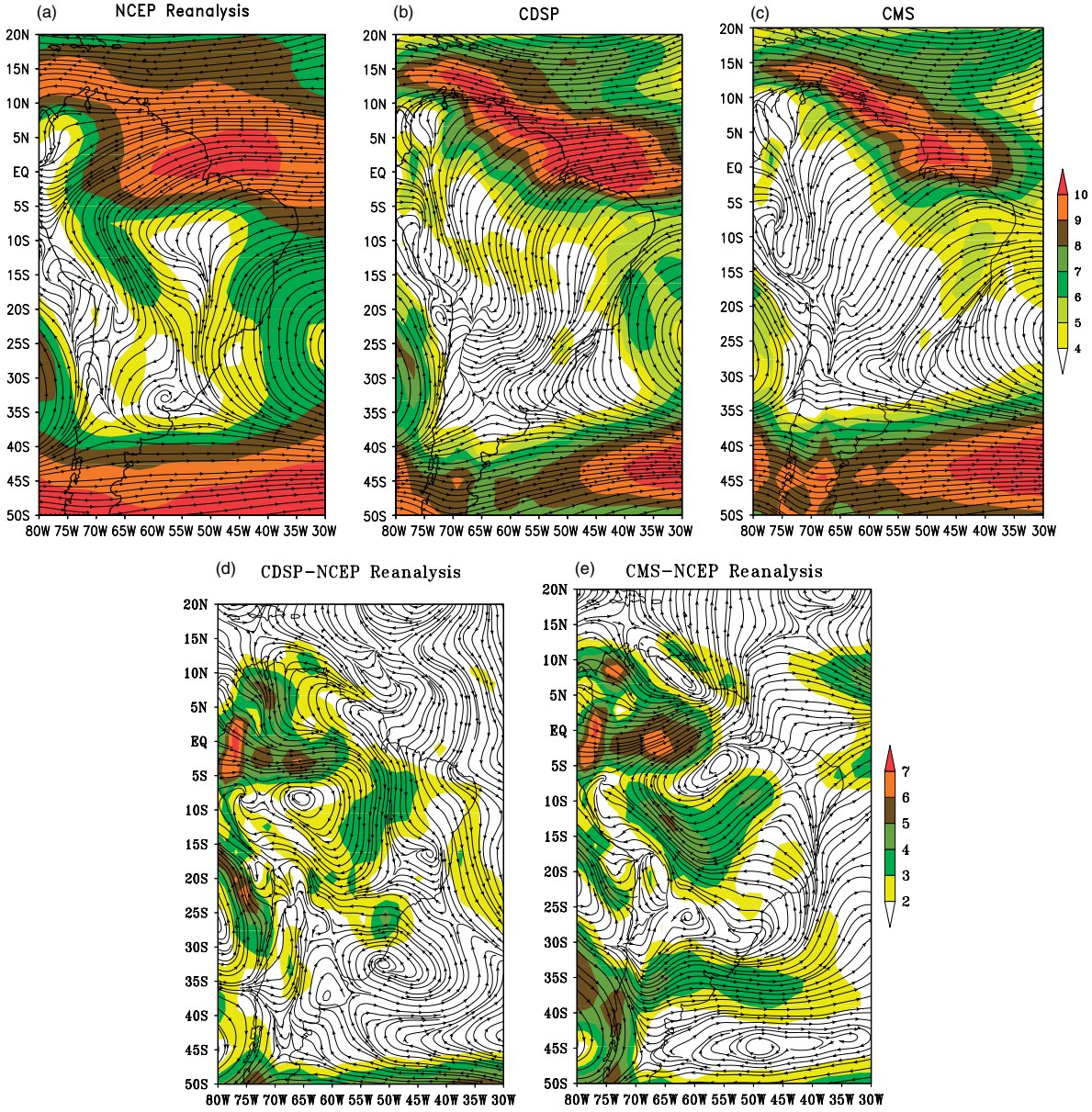

Figure 4. Same as Figure 2 but for 850 hPa circulation. Wind speed is shaded. The units are m s^{-1}. This figure is available in colour online at www.interscience.wiley.com/ijoc

by the CDSP and CMS are also seen (to a moderately lesser extent) in the NCEP-CFS (not shown) and in the Community Climate System Model Version 3.0 (CCSM3; Collins *et al.*, 2006; not shown). The corresponding SST differences from observations are shown in Figure 2(b) and (c). The cold tongue bias in the equatorial Pacific Ocean becomes more severe in the CMS compared to that in the CDSP. Furthermore, the subtropical SSTs in the CMS integration over the northern Atlantic Ocean also show some warm bias that effectively reduces the prevalent SST gradients relative to the CDSP and observations.

However, these precipitation and SST errors in the CDSP and the CMS integrations have implications on the low-level circulations of the SAM. In Figure 4(a)–(c), we show the climatological 850 hPa circulation from the NCEP reanalysis, the CDSP and the CMS integrations, respectively. Their corresponding differences from the NCEP reanalysis are shown in Figure 4(d) and (e), respectively. As a result of the relative reduction in the SST gradients over the tropical Atlantic Ocean in the CMS run, the cross-equatorial flow into tropical South America is comparatively weaker than either in the CDSP or in the NCEP reanalysis. Consequently, due to the reduction of the momentum of the cross-equatorial flow, the north-westerly flow along the eastern slopes of the Andes becomes much weaker in the CMS run compared to the CDSP integration and the NCEP reanalysis. Furthermore, the ridge along 7°S seen in the NCEP reanalysis (Figure 4(c)) which makes the observed climatological flow more north-westerly is poorly simulated in the model integrations.

We also examined the distribution of the daily precipitation in the DJF season over the SAM region from observations (rain gauge), CDSP and CMS model runs, as

DOI: 10.1002/joc

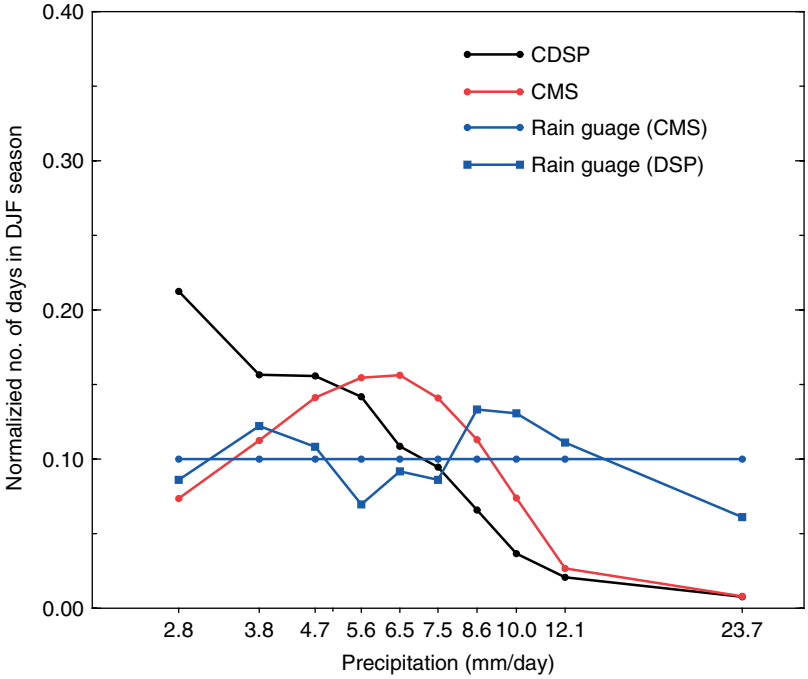

Figure 5. The distribution of the daily precipitation in December–January–February season over the SAM region. The frequency along the ordinate is normalized by the total number of days in the DJF season through the length of the corresponding dataset. The distribution rain gauge (CMS) corresponds to 40 years of observed data (Liebmann and Allured 2005; 1966–2005) while rain gauge (CDSP) corresponds to the same observed data but for 1982–83, 1988–89, 1997–98 and 1998–99. The ten bins along the abscissa are 0–2.8, 2.8–3.8, 3.8–4.7, 4.7–5.6, 5.6–6.5, 6.5–7.5, 7.5–8.6, 8.6–10.0, 10.0–12.1 and 12.1–23.7 mm day^{-1}. This figure is available in colour online at www.interscience.wiley.com/ijoc

shown in Figure 5. This distribution is normalized by the total number of days in the DJF season through the length of the dataset for easier comparison. Furthermore, the observed daily rain gauge data for the 40 years is divided into ten unequal bins such that each bin has an equal number of days (decile). We have also shown the observed daily distribution of precipitation data for the DJF season of 1982–1983, 1988–1989, 1997–1998 and 1998–1999 for comparison with the CDSP integration. From this Figure 5 it is apparent that the distribution of the daily precipitation over the SAM region in the CDSP and in the CMS integrations strongly overestimates (underestimate) the weak (strong) precipitation events relative to the observations. The difference in the climatological distribution of the daily precipitation between the CDSP and the CMS integrations relates to the spin-up of the tropical SSTs that result in a spin-down of the moisture field over tropical oceans, and a consequent reduction of precipitation over land surface (Larow and Krishnamurti, 1999; Kirtman *et al*., 2002). The distributions of daily precipitation from the CMS and CDSP were tested for their uniqueness using the Kuiper test (Press *et al*., 1986). The Kuiper test, tests against the null hypothesis that the two distributions were randomly selected from the same continuous probability distribution. Unlike other comparable tests, the Kuiper test has the more desirable property of being equally sensitive to differences at all points in the distributions, including the far side of the distribution tails. The tests proved the null hypothesis to be false at 99% confidence interval.

4.1.2. ii) Interannual variability

The teleconnection patterns depicted as the regressions of the mean DJF precipitation over continental South America from CMAP, rain gauge, CDSP and the CMS model runs on the corresponding mean DJF Niño3 SST index are shown in Figure 3(a)–(d), respectively. The CMAP (at 2.5° grid resolution) and rain gauge (gridded at 1° grid resolution) show some variations in this teleconnection pattern. The two datasets are somewhat consistent in showing insignificant relationship with ENSO over the SAM region. Significant ENSO relationship is seen over north-east Amazon and over south Brazil–Uruguay with opposite signs in both the observational datasets. Broadly, this teleconnection pattern is reasonably well captured by both the CDSP and the CMS integrations. For the CDSP integrations, we have strung out the ten ensemble members of each year so that we have a '40-year' long time series which is comparable with the CMS integration. Nonetheless, the ensemble members of the CDSP cannot be considered to be totally independent of each other. Therefore, we have used only 4 degrees of freedom (dof) to compute the significant values of the regression coefficients in Figure 3(c), unlike 40 dof used in the rest. There is, however, some difference in subtropical South America over Uruguay, with precipitation anomalies more dominant and significant in the CDSP. But, as shown in the Figure 3(d), these anomalies appear weakly as statistically insignificant values in the CMS as a result of the attenuation of this signal from weak ENSO events. If, however, this figure is redone using relatively strong

DOI: 10.1002/joc

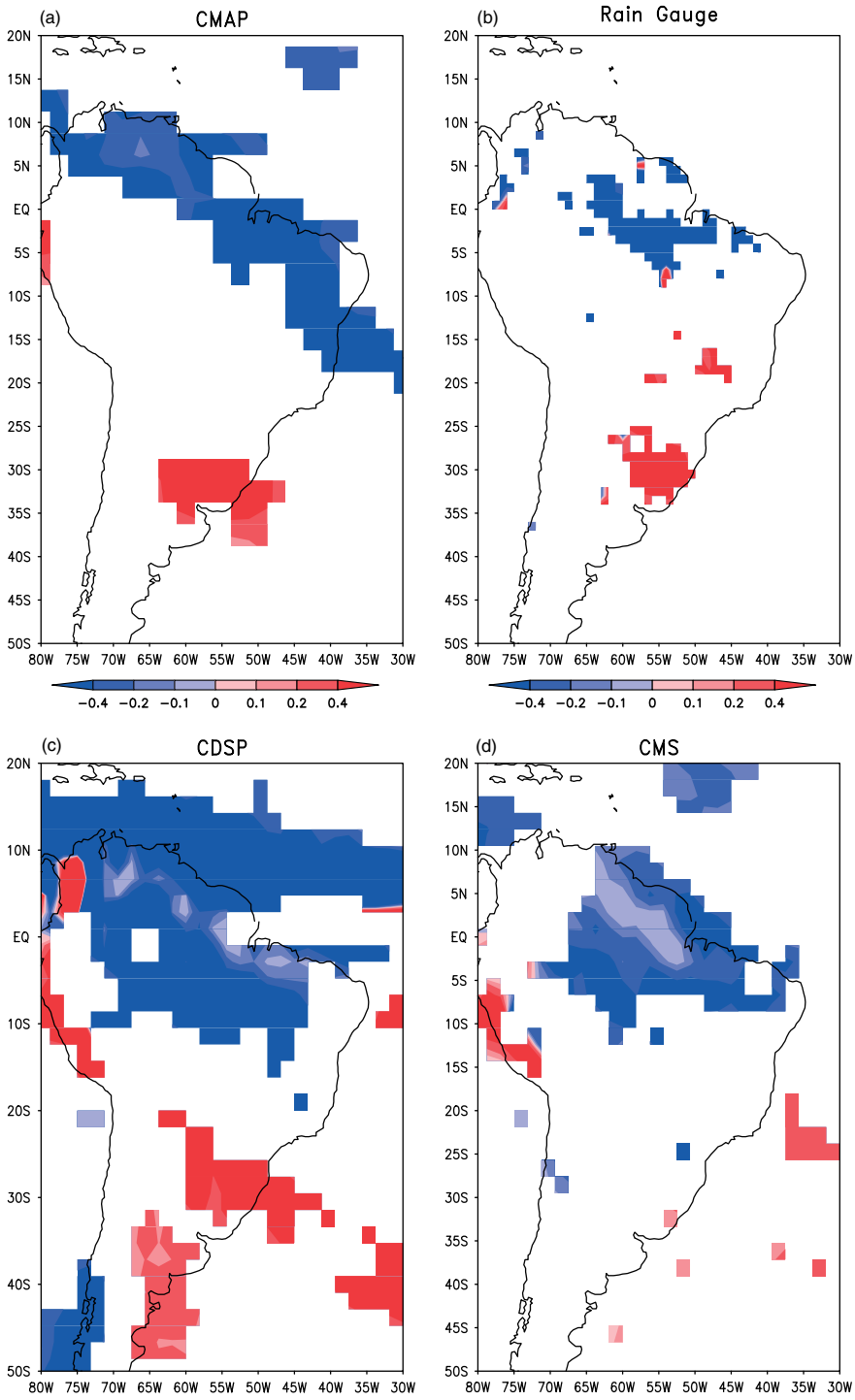

Figure 6. The regression of the mean DJF precipitation on the contemporaneous mean DJF Niño3 SST index over continental South America from (a) CMAP, (b) Rain Guage data (Liebmann and Allured 2005), (c) CDSP and (d) CMS. The SST in (a) and (b) is from HADISST1.1 (Rayner *et al*. 2002) while in (c) and (d) it is from the corresponding coupled model integration. Only significant values at 90% confidence interval according to *t*-test are plotted using 40 degrees of freedom (dof) in (a), (b) and (d) and 4 dof in (c). The units are in mm day^{-1}. This figure is available in colour online at www.interscience.wiley.com/ijoc

ENSO events that occur in the CMS integration, the precipitation anomalies appear as significant (not shown). It may however be pointed that the CDSP follows the CMAP regression pattern over south-east Brazil while the CMS does not indicate any significant relationship with the Niño3 SST index.

There are, however, some discrepancies between the two observed datasets like over central-east Brazil. Here, the CMAP (Figure 3(a)) shows negative as against the positive regression coefficients in the rain gauge data (Figure 3(b)). These positive regression coefficients of precipitation over central-east Brazil in relation to ENSO SST anomalies are, however, consistent with some of the past observational studies (Nogues-Paegle and Mo, 2002; Grimm, 2003, 2004). The CMS is unable to simulate any spatially coherent and significant relations over

DOI: 10.1002/joc

central-east Brazil, but the CDSP indicates some negative regression coefficients over central-east Brazil.

We have plotted the distribution of the daily precipitation for wet and dry SAM seasons in Figure 6. An SAM year is designated as wet if the DJF precipitation anomaly exceeds $0.5\times\sigma_p$ (where σ_p is the standard deviation of the corresponding mean DJF precipitation over the SAM region). Likewise, an SAM year is considered dry if the DJF precipitation anomaly is less than $-0.5\times\sigma_p$. This provides a reasonable sample of contrasting seasonal anomalies of DJF precipitation from the rain gauge data (Table 2). The rain gauge data in Figure 6(a) clearly show a shift in the distribution from strong to weak precipitation events in the wet and dry seasons, respectively. The CDSP runs show a marginal shift to relatively stronger events with some moderate reduction of the weakest precipitation event in going from a dry to a wet season in Figure 6(b). This frequency shift occurs comparatively over a broader range in the CMS integration in Figure 6(b) but is still much weaker than the observations in Figure 6(a). In Table 2, using the same criterion as used for the observations to distinguish between dry and wet monsoons, the CMS produces 15 wet and 11 dry seasons that compare well with the 26 anomalous seasons of the rain gauge data. In both the model runs (CDSP and CMS), the distribution of the daily precipitation in the wet and dry monsoon seasons is not as different from its climatological distribution as in the observations. In other words, the COLA model perceives the interannual variation as a vacillation of the daily precipitation events about its climatological distribution. In the rain gauge data, the largest change occurs at the tail ends of the distribution. The coupled model initialization seems to further exacerbate the model bias in the distribution of the daily precipitation. Each pair of distribution in Figure 6 passes the Kuiper test at 99% confidence interval.

Table II. Number of wet and dry DJF seasons of the South American monsoon.

Experiment Name	No. of Wet seasons	No. of Dry seasons
Rain gauge	11	14
CDSP, T62L64, T159L28, T159L64	2	2
CMS	15	11

4.2. Sensitivity experiments

The results from the various sensitivity runs outlined in Table 1 are discussed here. Primarily, these models differ in their AGCM resolution both in the vertical and in the horizontal. The OGCM is identical in all experiments. These experiments are motivated from the results of the CDSP and CMS integrations which suggest that the

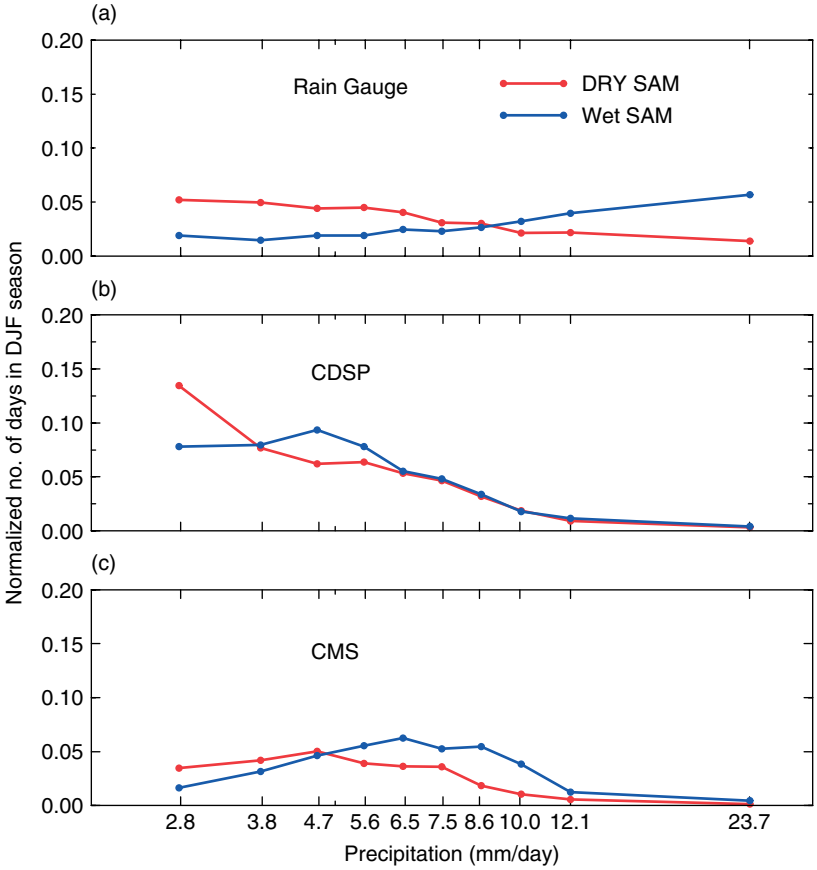

Figure 7. The distribution of the daily precipitation over the SAM region in DJF season in the dry (red) and wet (blue) SAM seasons from (a) Rain gauge (Liebmann and Allured 2005), (b) CDSP, and (c) CMS runs. The binning is as in Figure 5. This figure is available in colour online at www.interscience.wiley.com/ijoc

DOI: 10.1002/joc

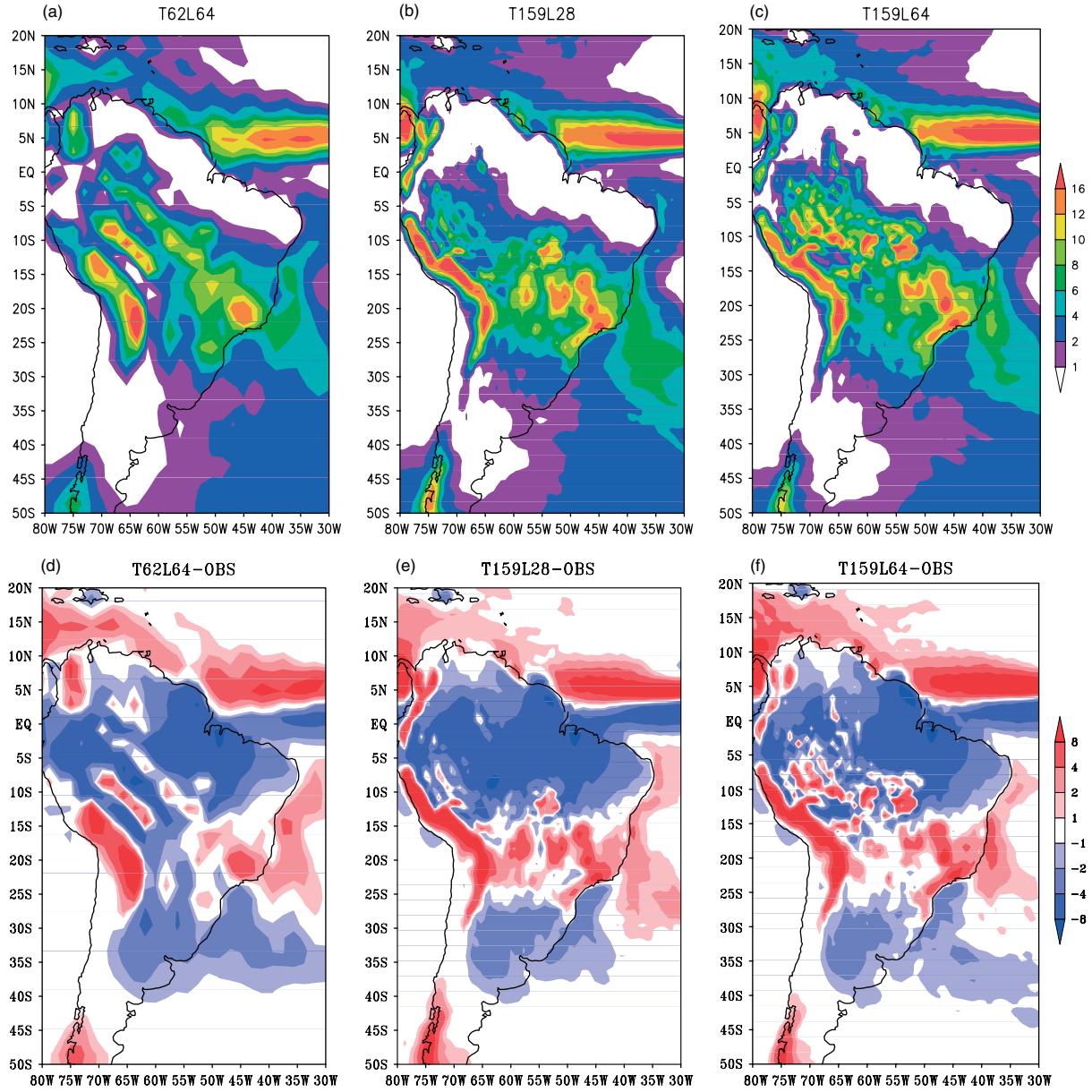

Figure 8. Same as Figure 2 but from sensitivity model runs (T62L64, T159L28 and T159L64). This figure is available in colour online at www.interscience.wiley.com/ijoc

resolution may be constraining the model from simulating stronger precipitation events.

4.2.1. *i) Climatology*

Similar to Figure 2 we have plotted the climatological seasonal mean DJF precipitation from the three sensitivity model runs in Figure 7. In comparison to Figure 2(b) and (d), the higher vertical resolution in the T62L64 integration (Figure 7(a) and (d)) yielded some reduction of the dry bias over the Amazon River Basin. But the precipitation errors over south-east Brazil and over central South America (Paraguay and north-eastern Argentina) in Figure 7(d) are nearly the same as in CDSP (Figure 2(d)). The higher horizontal resolution in the T159L28 experiment (Figure 7(b) and (e)) further exacerbated the dry bias over the central Amazon River Basin compared to CDSP and T62L64 integrations. But the banded structure of the precipitation on the leeward side of the Andes is reduced by the higher horizontal resolution of the T159 compared to the T62 spectral resolution. The wet bias over south-east Brazil and the Atlantic ITCZ region is further accentuated in the T159L28 seasonal hindcasts relative to the CDSP. At higher vertical resolution of T159L64 (Figure 7(c) and (f)), there is some significant reduction of the dry bias over the Amazon River Basin region relative to the rest of the seasonal hindcast sensitivity experiments. The excessive precipitation over the tropical Atlantic, a feature of all the seasonal hindcasts is further exacerbated at T159L64.

One of the obvious potential benefits of higher spatial resolution atmospheric models is that the orographic features are simulated better. At least, that is the conclusion drawn with respect to the low-level jet along the eastern slopes of the Andes from some of the previous studies

DOI: 10.1002/joc

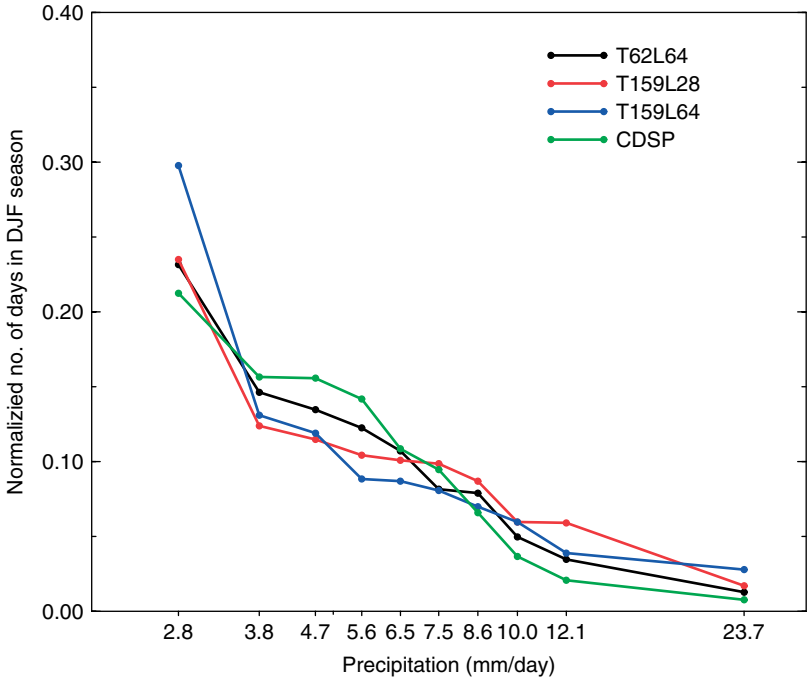

Figure 9. Same as Figure 5 but for the sensitivity runs (T62L64, T159L28 and T159L64). This figure is available in colour online at www.interscience.wiley.com/ijoc

that prescribed observed SST (Misra *et al*., 2002, 2003; Vernekar *et al*., 2003). However, as seen in Figure 7, the large precipitation errors over continental South America obviate the benefit of the higher resolution of the AGCM in the sensitivity runs. In these sensitivity runs, the low-level circulation of the cross-equatorial flow and the consequent north-westerly flow along the slopes of the Andes become much weaker than in the CDSP integration resulting in an apparent loss of resolving the low-level jet (not shown).

Similar to Figure 5, the distribution of the daily precipitation over the SAM region in the DJF season is shown in Figure 8 for the sensitivity experiments. The higher vertical resolution of 64 levels at T62 resolution had a marginal impact on the daily precipitation distribution compared to CDSP. The frequency of the stronger precipitation events increased slightly. The stronger precipitation events occur more often in both the T159 runs compared to their T64 counterparts. However, in all seasonal integrations the frequency of the strong precipitation events are far less than as suggested by the rain gauge data.

4.2.2. *ii) Interannual variability*

The regression of the mean DJF precipitation over continental South America corresponding to the mean DJF Niño3 SST index is shown for all the sensitivity runs in Figure 9. In comparison to the CDSP integration (Figure 3(b)), the interannual variations of the precipitation over south-east Brazil in the three sensitivity seasonal hindcast runs (T62L64, T159L28 and T159L64) are quite similar. Precipitation anomalies of opposite signs appear in all the seasonal hindcasts over tropical South America and subtropical South America (south Brazil and Uruguay). It may be concluded that the higher-resolution coupled seasonal hindcasts did not perceptibly improve the ENSO impact over South America. The higher horizontal resolution runs at T159 tend to shift the ENSO-related anomalies further westward over the Amazon relative to the CDSP, T62L64 integrations and rain gauge data.

In Figure 10, the distributions of the daily precipitation for the dry and wet SAM seasons are plotted as in Figure 6 for the sensitivity integrations. The T62L64 sensitivity run in Figure 10(a) exhibits a small improvement over the corresponding figure of CDSP in Figure 6(b) in that the daily precipitation events vary over a wider range of precipitation in the shift from an anomalous wet to dry season. The T159L28 runs in Figure 10(b) further improve upon T62L64 distribution, showing a small change in the tail end of the stronger events between the wet and dry seasons. The results from the T159L64 integrations in Figure 10(c) are quite similar to the T159L28 runs in Figure 10(b). Again, each pair of distribution in Figure 10 passes the Kuiper test at the 99% confidence interval.

5. Conclusions

In this study, we have examined the coupled ocean–atmosphere seasonal hindcasts of the SAM precipitation using the COLA-coupled climate model. It is seen that the climatology and variability of the SAM precipitation in the COLA-coupled model are not very different between a multi-decadal integration and a small set of comparable

DOI: 10.1002/joc

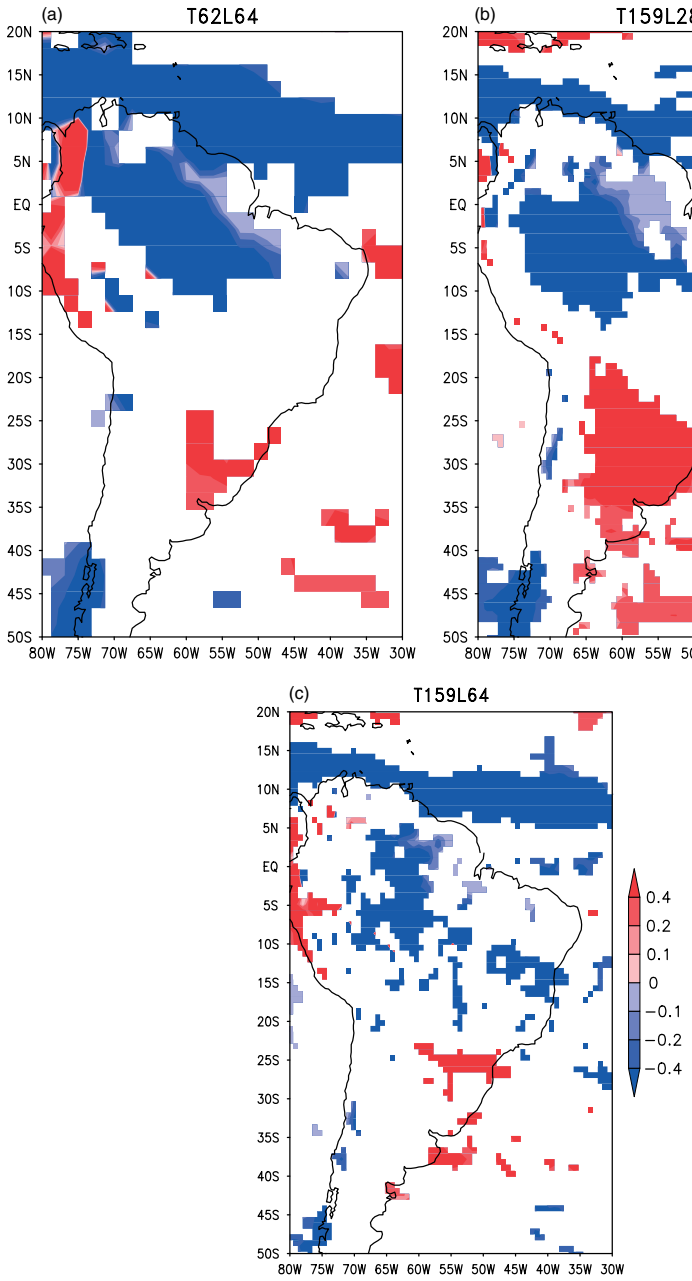

Figure 10. Same as Figure 6 but from the sensitivity seasonal hindcast runs (T62L64, T159L28 and T159L64) using only 4 dof to plot only the significant values at 90% confidence interval according to t-test. This figure is available in colour online at www.interscience.wiley.com/ijoc

seasonal hindcasts. Both modes of integration of the same model show the following:

1. Erroneous banded structure of the precipitation on the lee side of the Andes.
2. Dry bias the in northern part of continental South America and the Amazon.
3. Wet bias over south-east Brazil and atop central Andes.
4. Underestimation of strong events in daily precipitation totals over south-east Brazil.
5. Overestimation of weak events in daily precipitation totals over south-east Brazil.
6. Similar spatial pattern of precipitation anomalies over continental South America due to ENSO forcing.
7. Interannual variation of the daily precipitation totals over the SAM region is perceived as a vacillation about its climatological distribution in contrast to observations that show a distinct shift in its frequency distribution.

The subtle differences between the two model integrations relate more to the spin-down effect of the moisture field over land surface, which makes the dry bias over the Amazon and the northern part of South America more severe in the seasonal hindcast (CDSP) compared to the long-term simulation (CMS). Furthermore, the climatological distribution and its interannual variation of the daily precipitation over the core region of the SAM in the CMS appear to vary over a wider precipitation range

DOI: 10.1002/joc

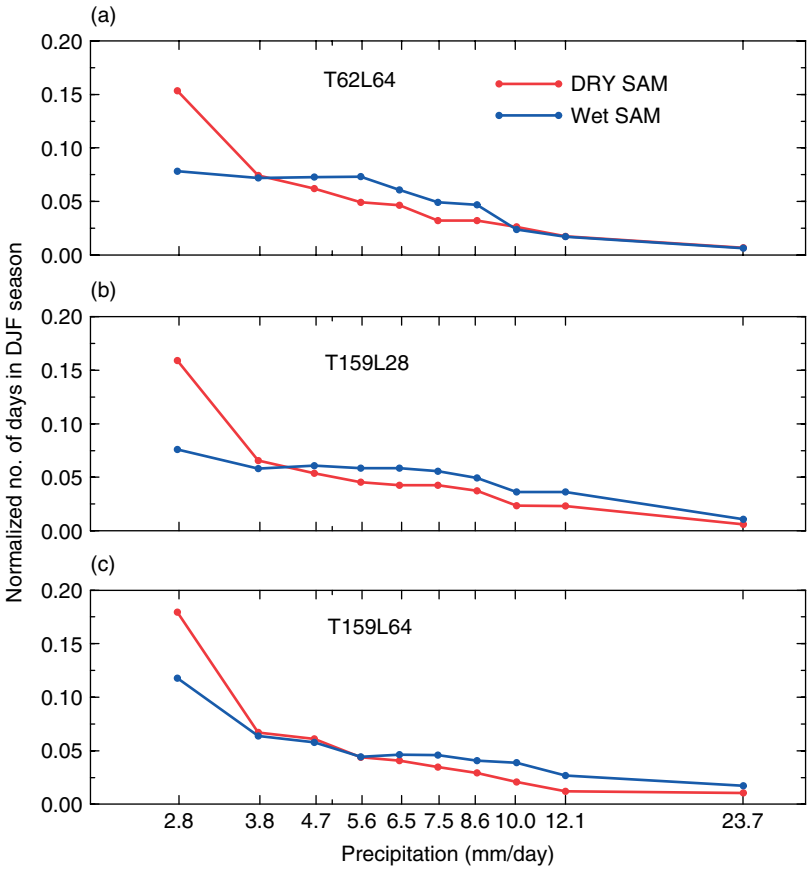

Figure 11. Same as Figure 7 but for the sensitivity seasonal hindcast runs (T62L64, T159L28 and T159L64). This figure is available in colour online at www.interscience.wiley.com/ijoc

than the CDSP. The Atlantic ITCZ also shows large differences between the two simulations. Furthermore, the relatively large warm bias of the subtropical SSTs in the north Atlantic Ocean in the CMS reduces the SST gradients. This results in weaker low-level cross-equatorial flow compared to that in the CDSP.

Three sensitivity experiments were conducted with three different resolutions of the AGCM component of the COLA-coupled climate model: T62L64, T159L28 and T159L64 (Table 1). The AGCM formulations differ only in the orography they use and the rate at which the energy is dissipated by the horizontal diffusion process. There is no significant change in the climatological mean DJF precipitation and in its interannual variability over continental South America between T159 and T62 resolution runs. However, the climatological distribution of the daily precipitation over the SAM core region shows some marginal improvement in the frequency of occurrence of heavy precipitation events. Likewise, the interannual variations in the frequency distribution of daily precipitation are marginally improved especially in the occurrence of heavy precipitation events in the wet monsoon year at T159 spectral resolution compared to T62.

The change in the vertical resolution of the AGCM in the COLA-coupled model did not have as comparable an impact as the change in the horizontal resolution which the AGCM had. This result is consistent with an earlier study of Bossuet *et al*. (1998) who also found insignificant impact on the mean climate of their model from changing the vertical resolution. The improvement in reducing the bias from changing resolutions in the COLA model is disappointingly much smaller than the model bias.

However, there are some important caveats of this study that need to be noted. First, these results could be model-dependent and will have to be examined in other models independently. Second, the choice of picking strong ENSO events for seasonal hindcast experiments is deliberate and may have an influence on the results of this study. However, this argument may have to be tempered by the fact that the current state-of-the-art coupled climate models may not be mature enough to provide reliable seasonal predictions under weak ENSO or near-neutral conditions in the eastern equatorial Pacific Ocean (Jin *et al*. 2008). Third, the resolution changes made to the AGCM from T62 (≈210 km) to T159 ((≈80 km) in this study are insufficient to make a case for drastic changes in the physics of the model. If however, for instance, we were to make a horizontal resolution change to resolve the meso-scale, then the physical parameterizations would have to be replaced with explicit physics. Under those circumstances it is not clear if the results of this study will be applicable.

DOI: 10.1002/joc

Acknowledgement

The authors would like to thank Drs Ben Kirtman and V. Krishnamurthy for their useful comments on an earlier version of the manuscript. We would also like to acknowledge the useful input of two anonymous reviewers. This study was supported by NSF Grant ATM0332910, NASA Grant NNG04GG46G and NOAA Grants NA04OAR4310034 and NA07OAR4310168. The use of computing resources at the NASA Ames facility under NASA project NNG06GB54G and Columbia project SMD05-0115 is also acknowledged.

References

Bacmeister JT, Pegion PJ, Schubert SD, Suarez MJ An atlas of seasonal means simulated by the NSIPP-1 atmospheric GCM. 17. NASA Tech Memo 104606. Goddard Space Flight Center, Greenbelt, 2000. 194.

Bossuet C, Deue M, Cariolle D. 1998. Impact of a simple parameterization of convective gravity-wave drag in a stratosphere -troposphere general circulation model and its sensitivity to vertical resolution. *Annales De Geophysique* **16**: 238–249.

Brankovic C, Gregory D. 2004. Impact of horizontal resolution on seasonal integrations. *Climate Dynamics* **18**: 123–143, DOI: 10.10007/s003820100165.

Carvalho LMV, Jones C, Liebmann B. 2004. The South Atlantic convergence zone: Intensity, form, persistence, and relationships with intraseasonal to interannual activity and extreme rainfall. *Journal of Climate* **17**: 88–108.

Chaves RR, Nobre P. 2004. Interactions between sea surface temperature over the South Atlantic Ocean and the South Atlantic Convergence Zone. *Geophysical Research Letters* **31**:, DOI: 10.1029/2003GL018647.

Collins WD, *et al*. 2006. The community climate system model version 3 (CCSM3). *Journal of Climate* **19**: 2122–2143.

Dirmeyer PA, Gao X, Zhao M, Guo Z, Oki T, Hanasaki N. 2006. Supplement to GSWP-2: details of the forcing data. *Bulletin of the American Society* **87**: S10–S16.

Dirmeyer PA, Zeng FJ. 1999. Precipitation infiltration in the Simplified SiB land surface scheme. *Journal of the Meteorological Society of Japan* **78**: 291–303.

Duffy PB, Govindswamy B, Iorio JP, Milovich J, Sperber KR, *et al*. 2003. High-resolution simulations of global climate, part I: present climate. *Climate Dynamics* **21**: 371–390, DOI:10.1007/s00382-003-0339-z.

Folland CK, Colman AW, Rowell DP, Davey MK. 2001. Predictability of northeast Brazil rainfall and real-time forecast skill., 1997 – 98. *Journal of Climate* **7**: 33–43.

Gent PR, McWilliams JC. 1990. Isopycnal mixing in Ocean circulation model. *Journal of Physical Oceanography* **25**: 150–155.

Grimm AM. 2003. The El Niño impact on the summer monsoon in Brazil: Regional processes versus Remote Influences. *Journal of Climate* **16**: 263–280.

Grimm AM. 2004. How do LaNiña events disturb the summer monsoon system in Brazil? *Climate Dynamics* **22**: 123–128.

Grimm AM, Barros VR, Doyle ME. 2000. Climate variability in southern South America associated with El Niño and La Niña events. *Journal of Climate* **13**: 35–58.

Grimm AM, Pal J, Giorgi F. 2007. Connection between spring conditions and peak summer monsoon rainfall in South America: Role of soil moisture, surface temperature, and topography in eastern Brazil. *Journal of Climate* **20**: 5929–5945.

Grimm AM, Vera C, Mechoso CR. 2005. *The South American Monsoon System. The Global Monsoon System: Research and Forecast Meteorology*, Chang C-P, Wang B, Lau NCG (eds). WMO/TD 1266: WMO: Geneva; 218–238, 542, Available online at http://www.wmo.int/pages/prog/arep/tmrp/REPORTS/global_monsoon_system_IMW3.pdf.

Hack JJ, Caron JM, Danabasoglu G, Oleson KW, Bitz C, Truesdale JE. 2006. CCSM-CAM3 Climate Simulation Sensitivity to Changes in Horizontal Resolution. *Journal of Climate* **19**: 2267–2289.

Hong SY, Pan HL. 1996. Nonlocal boundary layer vertical diffusion in a medium range forecast model. *Monthly Weather Review* **124**: 2322–2339.

Inness PM, Slingo JM, Woolnough SJ, Neale RB, Pope VD. 2001. Organization of tropical convection in a GCM with varying vertical resolution; implications for the simulation of the Madden-Julian Oscillation. *Climate Dynamics* **17**: 777–793, DOI: 10.1007/s00380000148.

Jin EK, KinterIII JL, Wang B, Park C-K, Kang IS, Kirtman BP, Kug JS, Kumar A, Luo J-J, Schemm J, Shukla J, Yamagata T. 2008. Current status of ENSO prediction skill in coupled ocean-atmosphere models. *Climate Dynamics*, In press , DOI: 10.1007/s00382-008-0397-3.

Kalnay E, *et al*. 1996. The NCEP/NCAR 40-year reanalysis project. *Bulletin of the American Society* **77**: 437–471.

Kiehl JT, Hack JJ, Bonan G, Boville BA, Williamson DL, Rasch PJ. 1998. The national center for atmospheric research community climate model: CCM3. *Journal of Climate* **11**: 1131–1149.

Kirtman BP. 2003. The COLA anomaly coupled model: ensemble ENSO prediction. *Monthly Weather Review* **131**: 2324–2341.

Kirtman BP, Fan Y, Schneider EK. 2002. The COLA global coupled and anomaly coupled ocean-atmosphere GCM. *Journal of Climate* **15**: 2301–2320.

Kobayashi C, Sugi M. 2004. Impact of Horizontal resolution on the simulation of the Asian summer monsoon and tropical cyclones in the JMA global model. *Climate Dynamics* **23**: 165–176, DOI: 10.1007/s00382-004-0427-8.

Krishnamurthy V, Misra V. 2007. Observed ENSO-South American Monsoon teleconnection. COLA Available from COLA, 4041 Powder Mill Road, Suite 302, Calverton, MD 20705 Technical Report 248, Available from ftp ://grads.iges.org/pub/ctr/ctr$_{248}$.pdf.

Large WG, McWilliams JC, Doney SC. 1994. Oceanic vertical mixing: A review and a model with a nonlocal boundary layer parameterization. *Reviews of Geophysics* **32**: 363–403.

Larow TE, Krishnamurti TN. 1999. Initial conditions and ENSO prediction using a coupled ocean-atmosphere model. *Tellus* **50A**: 76–94.

Liebmann B, Allured D. 2005. Daily precipitation grids for South America. *Bulletin of the American Society* **86**: 1567–1570.

Liebmann B, Jones C, de Carvalho LMV. 2001. Interannual variability of daily extreme precipitation events in the state of Sao Paulo, Brazi. *Journal of Climate* **14**: 208–218.

Misra V. 2004. An evaluation of the predictability of the austral summer seasonal precipitation over South America. *Journal of Climate* **17**: 1161–1175.

Misra V. 2006. Understanding the predictability of seasonal precipitation over northeast Brazil. *Tellus* **58A**: 307–319.

Misra V. 2007. A sensitivity study of the coupled simulation of the Northeast Brazil rainfall variability. *Journal of Geophysical Research* **112**: DOI:10.1029/2006jd008093.

Misra V, Dirmeyer PA, Kirtman BP. 2003. Dynamic downscaling of seasonal simulations over South America. *Journal of Climate* **16**: 103–117.

Misra V, Dirmeyer PA, Kirtman BP, Juang H-MH, Kanamitsu M. 2002. Regional simulation of interannual variability over South America. *Journal of Geophysical Research* **107**: DOI:10.1029/2001JD900216.

Misra V, Marx L. 2007. The manifestation of the remote response over equatorial Pacific in a climate model. *Journal of Geophysical Research* **112**: DOI:.10.1029/2007JD008597.

Misra V, *et al*. 2007. Validating and understanding ENSO simulation in two coupled climate models. *Tellus* **59A**: 292–308.

Misra V, Marx L, Fennessy M, Kirtman B, KinterIII JL. 2008 A comparison of climate prediction and simulation over Tropical Pacific.. *J. Climate*, **21**: 3601–3611.

Nobre P, Marengo JA, Cavalcanti IFA, Obregon G, Barros V, Camilloni I, Campos N, Ferreira AG. 2006. Seasonal-to-decadal predictability and prediction of South American Climate. *Journal of Climate* **19**: 5988–6004.

Nogues-Paegle J, Mo KC. 1997. Alternating wet and dry conditions over South America during summer. *Monthly Weather Review* **125**: 279–291.

Nogues-Paegle J, Mo KC. 2002. Linkages between summer rainfall variability over South America and sea surface temperature anomalies. *Journal of Climate* **15**: 1389–1407.

Pacanowski RC, Griffies SM. 1998. *MOM3.0 Manual*. NOAA/Geophysical Fluid Dynamics Laboratory: Princeton, NJ; 08542.

Press WR, Flannery BP, Teulosky SA, Vetterling WT. 1986. *Numerical Recipies: The Art of Super Computing*. Cambridge NOAA/GFDL University Press; 702.

Redi MH. 1982. Oceanic isopycnal mixing by coordinate rotate. *Journal of Physical Oceanography* **11**: 1443–1451.

Reynolds RW, Rayner NA, Smith TM, Stokes DC, Wang W. 2002. An improved in situ and satellite SST analysis for climate. *Journal of Climate* **15**: 1609–1625.

Rosati A, Gudgel R, Miyakoda K. 1997. The impact of ocean initial conditions on ENSO forecasting with a coupled model. *Monthly Weather Review* **125**: 754–772.

Saha S, *et al*. 2006. The NCEP climate forecast system. *Journal of Climate* **19**: 3483–3517.

Sampaio MJA. 2005. Brazil: Biotechnology and Agriculture to meet the challenges of increased food production, Available from http://www.cgiar.org/biotech/rep0100/Sampaio.pdf.

Smagorinsky J. 1963. General circulation experiments with the primitive equations: I. The basic experiment. *Monthly Weather Review* **91**: 99–164.

Tiedtke M. 1984. The effect of penetrative cumulus convection on the large-scale flow in a general circulation model. *Beitrage Physics Atmospheric* **57**: 216–239.

Vera C, Higgins W, Amador J, Ambrizzi T, Garreaud R, *et al*. 2006. Toward a unified view of the American Monsoon Systems. *Journal of Climate* **19**: 4977–5000.

Vernekar AD, Kirtman BP, Fennessy MJ. 2003. Low-level jets and their effects on the South American summer climate as simulated by the NCEP Eta Model. *Journal of Climate* **16**: 297–311.

Xie P, Arkin P. 1996. Analysis of global monthly precipitation using gauge observations, satellite estimates and numerical model predictions. *Journal of Climate* **9**: 840–858.

Xue Y-K, Sellers PJ, KinterIII JL, Shukla J. 1991. A simplified Biosphere Model for global climate studies. *Journal of Climate* **4**: 345–364.

Xue Y-K, Zeng FJ, Schlosser CA. 1996. SSiB and its sensitivity to soil properties. A case study using HAPEX-Mobilhy data. *Global and Planetary Change* **13**: 183–194.

DOI: 10.1002/joc